Polymer 51 (2010) 3213–3224

Contents lists available at ScienceDirect

Polymer

journal homepage: www.elsevier.com/locate/polymer

Elasticity and inelasticity of thermoplastic polyurethane elastomers: Sensitivity to chemical and physical structure

C.P. Buckley [a,*], C. Prisacariu [b], C. Martin [c]

[a] Department of Engineering Science, University of Oxford, Parks Road, Oxford OX1 3PJ, UK
[b] Institute of Macromolecular Chemistry "Petru Poni", Aleea Grigore Ghica Voda, Nr. 41A, Iasi 700487, Romania
[c] Manchester Materials Science Centre, University of Manchester, Grosvenor Street, Manchester M1 7HS, UK

ARTICLE INFO

Article history:
Received 6 December 2009
Received in revised form
27 April 2010
Accepted 29 April 2010
Available online 6 May 2010

Keywords:
Polyurethane
Elastomer
Mullins effect

ABSTRACT

Cyclic tensile responses of fourteen polyurethane elastomers were studied, with respect to their chemical composition and physical structure. Hard segment, soft segment and chain extender were varied, while keeping the hard segment fraction at ca 40% and soft segment molar mass at 2000 g/mol. Hard segments were generated from 4,4′-methylene bis(phenyl di-isocyanate) (MDI), or 4,4′-dibenzyl di-isocyanate (DBDI). Physical structure was characterized by X-ray scattering (SAXS and WAXS), revealing significant variations in degree of phase separation and degree of crystallinity, especially in the DBDI-based polymers. Large differences were found in the mechanical responses during first loading to a given strain. Tensile modulus and work input increased significantly with degree of hard phase crystallinity, but were independent of degree of phase separation. First cycle hysteresis was found to increase with reduced phase separation and with replacement of MDI by DBDI. In second and subsequent load cycles, however, in which the Mullins effect was observed, a remarkable degree of uniformity of response was discovered. A unique linear relation was obtained between second cycle hysteresis and second cycle work input, for all strain levels, and for all materials except for two (with highest phase separation) which showed slightly lower second cycle hysteresis. The results can be explained in terms of pull-out of segments from the hard phase on the first cycle, to form a new series-coupled soft phase, whose constitutive response then appears almost independent of chemical and physical structure.

1. Introduction

The thermoplastic polyurethanes (TPUs) are polymers with remarkable versatility. Through suitable choice of the di-isocyanates and diols combined in their synthesis, a huge range of physical properties is achievable. For example, these may be varied from those typical of soft elastomers to those of hard plastics, simply by varying the dominant diol from a flexible long-chain molecule to a small molecule such as ethylene glycol. This versatility is combined with the processing advantages of a thermoplastic. It is therefore understandable that TPUs are employed in an exceptionally wide range of manufactured products.

In polyurethane *elastomers*, resilience of the material is an important attribute. In many applications they are in commercial competition with other, relatively soft, elastomeric materials. The choice of material for any given application then hinges on a spectrum of key properties offered by relatively soft polymers – stiffness and strain recovery characterizing their elasticity, but also inelastic effects such as hysteresis and stress relaxation. In these respects the mechanical properties of thermoplastic polyurethane elastomers are similar to those of other thermoplastic elastomers. *First* loading to a given deformation is associated with higher stiffness and hysteresis than is typical for a homogeneous crosslinked elastomer. But the first loading causes damage to the microstructure, such that *subsequent* loading inside the envelope of previous deformations, is associated with lower stiffness and hysteresis. Consequently, re-loading follows a stress-strain path closer to the previous unloading path than to the first loading path: i.e. these materials typically exhibit the well-known Mullins effect [1–3].

An interesting feature of TPUs is that such behaviour is highly sensitive to the chemical and physical structures of the materials that are potentially under the control of the synthesist. For this advantage to be exploited more effectively, however, there is a need for deeper understanding of the mechanisms by which structure determines the properties of importance. The present work aims to advance this understanding, by means of a systematic study of the

* Corresponding author. Tel.: +44 (0) 1865 273156.
E-mail address: paul.buckley@eng.ox.ac.uk (C.P. Buckley).

0032-3861/$ – see front matter © 2010 Elsevier Ltd. All rights reserved.
doi:10.1016/j.polymer.2010.04.069

effects of varying chemical composition of a family of model TPUs on (a) their physical structure at the important nanometre length-scale, and (b) the resulting mechanical properties of interest.

Polyurethane elastomers are formed typically by reacting together three chemical constituents: a di-isocyanate (DI), a long-chain diol (or "macrodiol") (MD), and a small molecule chain extender (CE) diol. The resulting polymer may be considered a copolymer of the MD and DI-CE sequences: termed the soft segment (SS) and hard segment (HS) respectively, since the SS usually has its glass transition below ambient temperature and the HS is frequently a relatively rigid aromatic molecule with glass transition above ambient temperature. For the polymer to be genuinely thermoplastic, adventitious crosslinking by the action of absorbed moisture must be avoided [4,5] and this means the chemical composition expressed in numbers N of moles N_{DI}:N_{MD}:N_{CE} is constrained by stoichiometry $N_{DI} = N_{MD} + N_{CE}$. But dramatic variations in properties may be obtained by varying the ratio N_{DI}:N_{MD}, thereby changing the fraction of HS in the copolymer. However, the mechanical properties of TPUs are not only influenced by the HS fraction. In particular, since the DI is terminated at each end by urethane -NH-CO-O- linkages that are potentially able to hydrogen bond to corresponding groups on neighbouring molecules, mechanical properties will also depend on the extent to which this potential is realized.

In addition to chemical interactions, the physical arrangement of the molecules plays an important role. It is well-known that TPUs with the structure discussed above tend to exhibit phase separation – see, for example the review by Dietrich and Hespe [6]. It is energetically favourable for the SS and HS not to mix. Thus during cooling from above a critical order-disorder temperature, spontaneous segregation of SS and HS into separate soft (SS-rich) and hard (HS-rich) phases occurs by the process of spinodal decomposition. To achieve elastomeric performance, the SS must be the majority constituent by mass, and the phase structure then takes the form of discrete hard domains dispersed within a soft matrix. Such a phase structure impacts on mechanical properties, and a further structural parameter of importance, therefore, is the *degree* of phase separation. The overall mechanical properties depend upon the relative volume fractions of soft and hard phases, and on the intrinsic properties of each of the phases. These in turn depend on details of molecular packing of the constituents within the phases, including the density of hydrogen bonds. Crystallinity has been observed in the soft phase when the MD chain is long enough [4,6–9], and it is also sometimes present in the hard phase. The latter is usually limited to only a few percent for most HS structures when solidified from the melt, but there is one particular DI that, in the presence of a suitable CE, gives rise to significant degrees of crystallinity [2,10–12] and this is included in the present work (see below).

There have been several previous studies of the effects of varying HS fraction on the mechanical properties of TPUs. The purpose of the present work is to investigate the role of other important structural features, as summarized above. This is achieved by systematic variation of the three chemical constituents: DI, MD and CE. Two di-isocyanates are considered: the frequently employed 4,4′-methylene bis(phenyl di-isocyanate) (MDI), and its close relation 4,4′-dibenzyl di-isocyanate (DBDI), that is of special interest because of its tendency to crystallize on cooling from the melt in the presence of some chain extenders [10–13]. Three macrodiols are considered: poly(ethylene adipate) (PEA), polytetrahydrofuran (PTHF), and poly(butylene adipate) (PBA). These were chosen because polyethers such as PTHF are well-known to promote phase separation from the DI, while polyesters such as PEA and PBA have a greater affinity for the DI through hydrogen bonding to their ester groups and hence are more miscible with the DI and phase segregation is expected to be less pronounced [4,14]. Three chain extenders are considered: ethylene glycol (EG), diethylene glycol (DEG) and 1,4 butylene glycol (BG). These were selected so as include two CEs that promote crystallinity with DBDI (EG and BG), and DEG that has been shown previously to inhibit crystallinity in DBDI [11].

Results are reported here for a set of 14 model TPU materials prepared with differing combinations of DI, MD and CE, but all having approximately the same mass fraction of HS (ca 40%), and all having soft segments of the same molar mass (2000 g/mol). As expected, the differing chemical compositions of the TPUs caused variation in the degree of phase separation and crystallinity. These were characterized by small-angle X-ray scattering (SAXS) and wide-angle X-ray scattering (WAXS) respectively.

The materials were subject to a series of cyclic uniaxial tensile tests at room temperature and ambient humidity, designed to characterize features of their constitutive response relevant to their performance as thermoplastic elastomers, especially focusing on their stiffness and their deviations from purely elastic behavior. A preliminary report of the work has already appeared [2], in which some of the results were summarized. In particular, a surprising feature noted there was an unexpected conformity in the relative second cycle hysteresis right across the range of materials. The present paper gives a full account of the results, and offers physical explanations for the effects observed, in terms of the structural evolution of TPU elastomers during deformation.

2. Experimental methods

2.1. Materials

The family of model TPUs was synthesised for this work in the authors' Romanian laboratory. As outlined above, they were all three-component systems combined in stoichiometric proportions, and consisting of: (1) a di-isocyanate – either MDI or DBDI; (2) a macrodiol MD – PEA, PTHF, or PBA; and (3) a small molecule diol as chain extender CE – anhydrous EG, DEG, or BG. The macrodiols were all of molar mass $M_w = 2000 \pm 50$ g mol^{-1}. The three components were always mixed in the molar proportions HS:MD:CE = 4:1:3, giving hard segment mass fractions in the region of 40%, and isocyanic index $I = 100$. Synthesis was carried out by the pre-polymer route described previously by Prisacariu et al. [10,11]. The DI and MD components were reacted together with vigorous mixing under vacuum at 100 °C, to give pre-polymer consisting of MD terminated at each end by DI. This was then thoroughly mixed with the CE at 90 °C, and cast into closed sheet moulds for curing at 110 °C over 24 h. The final result was polymer with M_w in the range 60–120 kg mol^{-1}, in the form of sheets with thickness in the range 0.3–0.6 mm. The sheets were stored at room temperature for at least one month before testing. They were labeled Pu1–Pu14 according to their combination of HS, MD and CE, as indicated in Table 1. It should be noted that the stoichiometric proportions used in these polymers ($I = 100$) means that they are truly thermoplastic. They do not have the potential for further reaction with ambient humidity to produce chain lengthening and allophanate cross-linking, seen in similar polymers but with excess isocyanate groups (e.g. $I = 110$) [5,10].

2.2. Structure studies

Information on the nanometre-scale physical structures of the materials was gained by X-ray scattering, using synchrotron radiation at the UK Daresbury Laboratory. Wide-angle X-ray scattering (WAXS) studies were carried out using Station 16.2 SMX, with X-ray

Table 1
Chemical and physical structures of the TPUs studied in this work. Q is the relative SAXS scattering invariant obtained from the intensity distribution, d is the dominant long period obtained from q^* the position of the peak SAXS intensity, A/V is the particle surface-to-volume ratio obtained from SAXS, and χ is the degree of crystallinity as determined from WAXS.

Material	DI	MD	CE	Hard segment volume fraction φ_H	Q	d nm	A/V nm^{-1}	χ
Pu1	MDI	PEA	EG	0.356	0.82	–	–	0.036
Pu2	MDI	PEA	DEG	0.380	2.46	18.7	0.722	0
Pu3	MDI	PEA	BG	0.372	2.30	14.1	0.816	0
Pu4	DBDI	PEA	EG	0.363	5.69	16.0	0.822	0.165
Pu5	DBDI	PEA	DEG	0.387	2.32	22.0	0.721	0
Pu6	DBDI	PEA	BG	0.378	2.47	16.8	0.659	0.104
Pu7	MDI	PTHF	EG	0.326	28.69	21.0	0.441	0.012
Pu8	MDI	PTHF	DEG	0.350	11.40	22.8	0.572	0
Pu9	DBDI	PTHF	EG	0.333	34.35	18.7	0.753	0.158
Pu10	DBDI	PTHF	DEG	0.356	22.91	20.1	0.519	0
Pu11	MDI	PBA	EG	0.323	5.64	18.7	0.586	0
Pu12	MDI	PBA	BG	0.338	5.47	16.8	0.835	0.027
Pu13	DBDI	PBA	DEG	0.344	4.96	–	0.536	0
Pu14	DBDI	PBA	BG	0.354	6.28	16.2	0.556	0.183

wavelength 82 pm. The 2D patterns were radially averaged to produce 1D intensity profiles. In some of the materials, predominantly some of those based on DBDI, sharp peaks were observed in the WAXS intensity versus 2θ scans, indicating some crystallization of the hard segments. There was no indication of crystallinity arising from the soft segments in these materials. The scattering intensity was separated into amorphous halo (I_a) and crystal diffraction (I_c) components by fitting Gaussian peaks to those crystal diffraction peaks visible, following the procedure used in a previous paper [10], and a degree of crystallinity χ was determined from the ratio of the integrated intensities:

$$\chi = \int I_c d\theta / \int (I_a + I_c) d\theta \quad (1)$$

Values of χ are included in Table 1.

Small-angle X-ray scattering (SAXS) studies were carried out using Daresbury Station 16.1 with the RAPID 2-dimensonal detector, with X-ray wavelength $\lambda = 141$ pm and a camera length of 4 m. Scattering intensities were radially averaged, to obtain 1-D patterns of intensity versus $q = (4\pi/\lambda)\sin\theta$. Three features are of particular interest.

Firstly, wide variations were observed in the scattering intensity for different materials, indicating differing degrees of phase separation. This was quantified as follows, following Saiani et al. [15]. For each scattering pattern, the measured intensity (in arbitrary units) was normalized for specimen thickness and incident beam intensity. Then the high q tail of the curve of normalized intensity $I_n(q)$ was fitted to Porod's Law for scattering by a two-phase system with sharp phase boundaries $I_n = K/q^4 + I_b$. Excellent agreement was found in all cases except Pu1. For the other polymers the mean R^2 for fitting to Porod's Law was 0.996. These fits provided the background intensity I_b (assumed independent of q) and Porod constant K. The corrected intensity $I = I_n - I_b$ was then employed in determining the relative scattering invariant Q from the relation.

$$Q = \int_0^\infty q^2 I(q) dq \quad (2)$$

where the upper end of the range of integration, beyond where data were available, was obtained with the extrapolation $I = K/q^4$.

Secondly, all but two of the scattering patterns obtained showed a distinct peak, at a position q^* in the region of 0.3 nm^{-1}. In these cases, a "long period" d was calculated from $d = 2\pi/q^*$, representing a dominant repeat distance of the two-phase structure causing the scattering.

Finally, the availability of both parameters K and Q enabled another structural measure to be estimated: the particle surface area-to-volume ratio A/V. It was obtained as follows [16]

$$A/V = \frac{\pi K}{Q}(1 - \varphi_h) \quad (3)$$

where φ_h is the volume fraction of particles: hard DI-rich domains in the present materials. Note that φ_h could only be approximated, since the exact composition and densities of particles and matrix are unknown. In applying equation (3), it was approximated by its theoretical limit in the case of complete phase segregation, i.e. the hard *segment* volume fraction φ_H, calculated from the hard segment mass fraction, the density of the hard segments (taken to be 1.29 g/ml for DBDI and 1.27 g/ml for MDI [15]), and the density of the soft segments (taken as 1.18 g/ml for PEA, 1.04 g/ml for PTHF and 1.02 g/ml for PBA).

Values of φ_H, Q, d and A/V are included in Table 1.

2.3. Mechanical tests

The sheet materials of thickness 0.3–0.6 mm were cut into rectangular strips of width 6 mm, and tested in uniaxial tension at ambient temperature (23 ± 1 °C) and humidity (41 ± 7% RH) using an Instron model 4204 testing machine at Oxford, with 50 mm between the grips. Extension was measured in the centre of the specimen using an Instron "Elastomer" model potentiometric extensometer, with a gauge length of 20 mm, with a data capture rate of 10/s. No strain localization was detected within the guage length. The experimental programme was divided into two phases, with a different experimental protocol in each phase. The resulting data are expressed below in terms of nominal stress s and nominal strain e.

Phase 1 consisted of three load-unload cycles to a maximum nominal strain $e_{max} = 3$, using a constant nominal strain-rate of magnitude 0.03 s^{-1}. No dwell time was allowed when the straining changed direction. From the stress-strain data obtained, several properties of interest were determined. The tensile modulus E was calculated as the gradient ds/de at $e = 0.01$, determined by fitting a quadratic function to the stress-strain curve over the strain range 0.005–0.015 and differentiating analytically. The values quoted below are means over an average of 4.5 samples for each material, and in each case the standard error of the mean was 2.4 MPa or less. Assuming linear viscoelasticity, this value of E corresponds to the isochronal 0.3s tensile stress relaxation modulus. Also determined was the residual strain on first unloading e_r, expressed as relative

residual strain $e_r^* = e_r/e_{max}$. In addition, the data were used to compute various measures of specific work input W, obtained by the integration $W = \int s de$. The first cycle work input W_1 was obtained by integration over the first loading up to e_{max}; first cycle hysteresis ΔW_1 by integration over the whole first load-unload sequence; second cycle work input W_2 by integration over the second loading, from e_r to e_{max}; and second cycle hysteresis ΔW_2 by integration over the whole second load-unload sequence. The reproducibility of these work calculations was better than 8% in all cases. In comparing the materials, it was convenient to express ΔW_1 as the relative first cycle hysteresis $\Delta W_1^* = \Delta W_1/W_1$

Phase 2 consisted of a series of load-unload cycles conducted at the same rate as in Phase 1, but taken to progressively higher nominal strains e_{max} on each cycle: 1, 2, 3…. Between 3 and 5 cycles were possible before failure with most materials. These may be described as 'pseudo-cyclic' experiments, to distinguish them from those in Phase 1 where the maximum strain was constant. As in Phase 1, for each value of e_{max}, the second cycle work input W_2 was obtained by integrating over the second loading from e_r to e_{max}. In this phase, however, the second cycle to any particular e_{max} was left incomplete, since straining continued to the next value of e_{max}. Therefore the second cycle hysteresis ΔW_2 was approximated by integrating over the first unloading from e_{max} and the second loading to e_{max}, and we shall distinguish it in the following with the notation $\Delta W_2'$. In this way, for each material, a series of values of W_2 and $\Delta W_2'$ was obtained, for various values of e_{max}.

3. Results and interpretation

3.1. Structural studies

It is well-known that block copolymers such as those studied here have a tendency to phase separation. Fig. 1 shows SAXS patterns for eight of the materials, providing evidence of phase separation in the present series of materials. But Fig. 1 also reveals that the SAXS intensity, indicating the degree of phase separation, varies greatly between the materials. In particular, it is clearly visible that the polymers with strongest scattering are those with PTHF as macrodiol. This result is quantified in Table 1, where the values of relative scattering invariant Q provide numerical measures of the relative degree of phase separation, since it depends on the hard phase volume fraction φ_h and the difference in electron density (ρ_e) in hard (h) and soft (s) phases as follows [15]

$$Q \propto \varphi_h(1-\varphi_h)(\rho_{e,h}-\rho_{e,s})^2. \quad (4)$$

In the arbitrary units of Q in Table 1, the PTHF-based polymers Pu7, Pu8, Pu9 and Pu10 have Q in the range 11–34, while all the other polymers have smaller values in the range 0.8–6.

The observation that PTHF-based TPUs phase-separate to a greater extent than the corresponding PEA and PBA-based polymers is consistent with previous studies of polyurethanes, that showed polyether macrodiols to give greater phase separation than polyester macrodiols [4,14]. The reason is believed to be the availability of a >C = O group on each monomer in a polyester for possible hydrogen bonding with the >N–H groups on the hard segments. This lowers the free energy of mixing of hard and soft segments that drives phase separation, relative to those macrodiols where this is absent, such as the polyethers.

Fig. 1 also shows that the SAXS patterns of most polymers had pronounced peaks in intensity, indicating a dominant repeat distance for the 2-phase structure. As quantified by the long period d, this varied from 14 to 23 nm. Such values for d and the values of hard domain area-to-volume ratio A/V, listed in Table 1, emphasise the small sizes of the domains. An important consequence for the mechanical properties of the materials is that a large fraction of the hard segment monomers must therefore reside at the surfaces of the domains. This fraction may be quantified in terms of $v^{1/3}A/V$ where v is the volume of one hard segment monomer. In the present materials the fraction varies between ca 32% (Pu7) to 62% (Pu12). Finally, another notable implication is that molecular mobility within the soft matrix must suffer significant constraint from the excluded volume of the hard domains. An approximate measure of the average width of the gap between domains may be obtained from $(V/A)(1-\varphi_H)/\varphi_H$. The values in Table 1 indicate that this quantity varies between 2.1 nm (Pu3) and 4.6 nm (Pu14). In addition, mobility in the soft phase must be reduced by their molecular connection to the relatively immobile segments of the hard domains.

WAXS patterns gave evidence of hard phase crystallinity in some of the materials. Fig. 2 illustrates the range of types of pattern

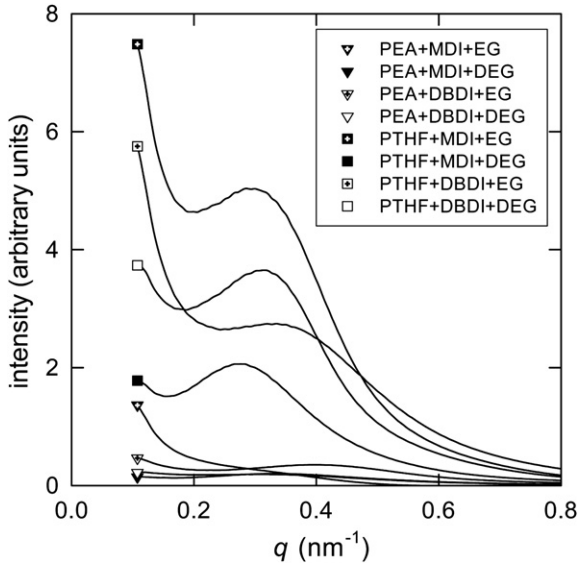

Fig. 1. Example 1-D SAXS patterns normalized and baseline-corrected as described in the text, for eight of the materials listed in Table 1, with compositions shown.

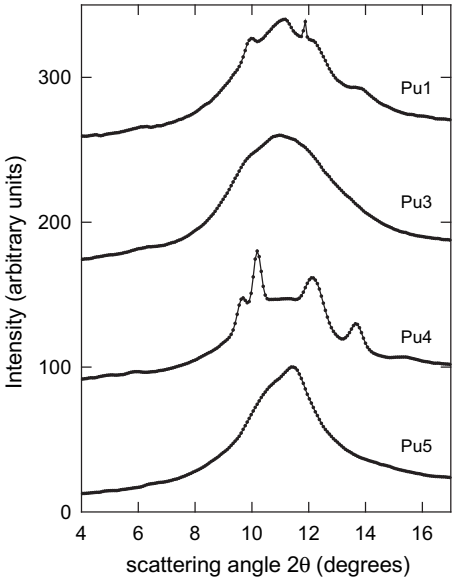

Fig. 2. Example 1-D WAXS patterns for four representative materials: all are based on PEA as macrodiol but differ in di-isocyanate and chain extender. Pu1 (MDI + EG) is slightly crystalline (4%), Pu3 (MDI + BG) is amorphous, Pu4 (DBDI + EG) is significantly crystalline (17%), Pu5 (DBDI + DEG) is amorphous. Consecutive patterns have been shifted vertically 80 units for clarity.

obtained: DBDI-based polymers with intense sharp peaks indicating significant crystallinity (Pu4), DBDI-based polymers with no sharp peaks indicating no crystallinity (Pu5), MDI-based polymers with low intensity sharp peaks indicating very slight crystallinity (Pu1), and MDI-based polymers showing only an amorphous halo (Pu3).

Table 1 includes the degree of hard segment crystallinity χ for all the materials. It is notable that all the MDI-based polymers show no, or only slight, crystallinity (maximum 4%). The only polymers to have more significant crystallinity are those based on DBDI. This is consistent with previous reports of comparisons between melt-processed polyurethanes based on these two di-isocyanates [10,13]. But the presence of DBDI does not always lead to crystallinity: it depends on the choice of chain extender. In Table 1, the DBDI-based polymers with DEG as chain extender can be seen to have no detectable crystallinity, whereas those with EG and BG have degrees of crystallinity up to 18%.

The relative ease of crystallization in DBDI as compared to MDI is readily explained in terms of greater flexibility of the DBDI molecule, arising from its $-(CH_2)_2-$ bridge between the phenyl rings, compared to only $-CH_2-$ in MDI [10,13]. Thus DBDI hard segments can adopt a linear conformation facilitating packing and inter-chain hydrogen bonding. MDI hard segments, however, are intrinsically kinked in shape, reducing conformational mobility and thereby hindering close packing and achievement of hydrogen bonding [10,13]. Conversely, when DEG is used as chain extender with DBDI, the central $-O-$ atom introduces kinks into the DBDI hard segment and disrupts the chain packing that could otherwise be achieved [11].

3.2. Mechanical tests – Phase 1

Example stress-strain curves obtained are shown in Fig. 3, where the directions of straining are indicated by arrows. The three curves shown exemplify the response seen with non-crystalline MDI-based TPUs (Pu2), with semicrystalline DBDI-based TPUs (Pu6), and with non-crystalline DBDI-based TPUs (Pu10). Several features are apparent immediately.

All three materials show pronounced hysteresis, and all three cyclic responses exhibit the well-known Mullins effect, whereby in second loading to a given strain a material follows a stress-strain path closer to the previous *unloading* path than to the first *loading* path. Comparing the curves in Fig. 3, we may also see consequences of differing chemical structures, that were replicated across the whole set of materials. Firstly it is clear that material Pu2 (MDI-based) has a discernibly lower initial stiffness than the other two materials (DBDI-based). Secondly the hysteresis and residual strain in the case of Pu6 (semicrystalline and DBDI-based) are significantly greater than in the case of both the other two materials (non-crystalline and either MDI or DBDI-based). Thirdly, material Pu2 shows significantly more strain hardening than the two DBDI-based materials.

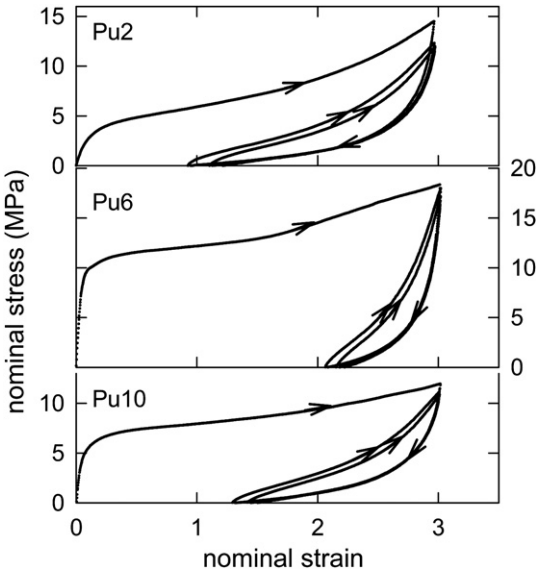

Fig. 3. Examples of stress-strain curves obtained in the 3-cycle load-unload tensile tests of Phase 1. Arrows indicate the direction of straining. Nominal strain-rate = 0.03 s^{-1}.

The four parameters used to characterize the first and second load/unload cycles are collected in columns 2–5 of Table 2. Materials Pu9 and Pu11 are missing (except for the measurement of modulus), since they were insufficiently ductile to withstand cyclic straining to $e = 3$.

3.2.1. Tensile modulus

Consider first the isochronal tensile modulus $E(0.3s)$. It varies widely between 39 and 324 MPa. But within this range there is a clear pattern. In every case, the modulus of MDI-based materials (maximum value 86 MPa) is lower than that of DBDI-based materials (minimum value 122 MPa). Moreover, the modulus of those DBDI-based materials without crystallinity (maximum value 138 MPa) is always lower than that of DBDI-based materials with crystallinity (minimum value 185 MPa). It is informative also to consider how the modulus depends on physical structure of the polymers. In Fig. 4 the modulus is plotted versus Q, quantifying the degree of phase separation, for all the materials. It shows clearly that the modulus is independent of Q when the degree of phase separation varies through change of macrodiol, while DI and CE are unchanged. Fig. 5, however, shows the modulus plotted versus degree of crystallinity. This shows clearly that the modulus does increase with increasing degree of crystallinity in the DBDI-based materials, *and* that in addition there is the purely chemical effect mentioned above: DBDI always gives a polymer with higher modulus than MDI, irrespective of choice of CE and MD.

How can such large variations in tensile modulus be explained within a family of TPUs where the hard segment concentration is almost constant and the soft segment chain length is constant? They are two-phase materials: HS-rich hard domains are surrounded by a continuous SS-rich soft matrix. But there is likely to be, in general, some phase mixing (HS occurring in the matrix and SS occurring in the hard domains). In interpreting physical properties of such a system, some insight can be gained by considering it as a particulate composite material, comprising two phases each of which has *effective* continuum properties such as elastic constants. Applying this approach to the present TPU systems, there are three possible sources of variation in elastic constants: variation of the hard phase volume fraction φ_h, variation of elastic constants of the soft matrix, and variation in elastic constants of the hard particles. Here, to make the problem tractable we invoke two, physically reasonable, approximations: (1) both phases are isotropic elastic continua; (2) the TPU elastomers are incompressible – i.e. Poisson's ratio $\nu = 0.5$.

To understand the variation of tensile modulus of such a system requires a solution to the well-known problem of predicting elastic constants of a 2-phase material. In general there is no analytical solution to this problem. The only rigorous predictions for arbitrary particle shape are bounds on the bulk and shear modulus – the tightest bounds are those proposed by Hashin and Shtrikman [17]: see for example the review by Christensen [18]. For the present materials, however, (one phase rubbery and the other glassy or crystalline) the bounds are likely to be rather too far apart to be useful. A convenient empirical description that lies approximately

Table 2
Tensile test results for first and second loading/unloading cycles to nominal strain $e = 3$. Test temperature = 23 ± 1 °C, relative humidity = 41 ± 7% RH, and nominal strain-rate = 0.03 s^{-1}.

Material	1st cycle tensile modulus E (MPa)	1st cycle work input W_1 (MJm^{-3})	1st cycle relative hysteresis ΔW_1^*	1st cycle relative residual nominal strain e_r^*	2nd cycle work input W_2 (MJm^{-3})	2nd cycle hysteresis ΔW_2 (MJm^{-3})
Pu1	85.7	28.2	0.834	0.463	9.61	5.14
Pu2	45.0	22.5	0.788	0.323	9.51	5.05
Pu3	47.3	28.2	0.829	0.416	10.3	5.57
Pu4	324	50.1	0.910	0.586	9.64	5.32
Pu5	138	19.2	0.889	0.516	4.11	2.08
Pu6	185	40.8	0.924	0.690	6.34	3.35
Pu7	70.5	29.8	0.757	0.246	11.7	5.35
Pu8	39.2	26.7	0.744	0.228	11.8	5.52
Pu9	305	–	–	–	–	–
Pu10	125	26.3	0.855	0.435	7.31	3.61
Pu11	74.3	–	–	–	–	–
Pu12	72.9	34.8	0.857	0.524	11.0	6.28
Pu13	122	24.8	0.904	0.681	5.09	2.82
Pu14	250	45.6	0.939	0.747	5.72	3.15

mid-way between the bounds is the log-law used by Gray and McCrum in interpreting the dependence of shear modulus on degree of crystallinity in polyethylene [19]. Applied to the present TPUs, this gives the shear modulus G as follows.

$$\ln G = \varphi_h \ln G_h + (1 - \varphi_h)\ln G_s \tag{5}$$

where G_h and G_s are shear moduli of hard and soft phases respectively. Hence the tensile modulus of the composite can be obtained from $E = 2G(1 + \nu)$. Two interesting results follow.

Firstly, suppose there is some phase mixing. Let a fraction f_{hs} of the hard segments mix into the soft matrix and a fraction f_{sh} of the soft segments mix into the hard particles. Suppose also that equations analogous to equation (4) apply also to the shear moduli of the individual phases, in terms of shear moduli G_H and G_S intrinsic to the hard segments and soft segments respectively. Then there are two additional equations giving the hard and soft phase shear moduli in terms of the hard segment volume fraction ϕ_H:

$$\begin{aligned}\ln G_h &= \varphi_h^{-1}[\varphi_H(1-f_{hs})\ln G_H + (1-\varphi_H)f_{sh}\ln G_S];\\ \ln G_s &= (1-\varphi_h)^{-1}[\varphi_H f_{hs}\ln G_H + (1-\varphi_H)(1-f_{sh})\ln G_S].\end{aligned} \tag{6}$$

Combining equations (5) and (6), gives the shear modulus in terms of intrinsic hard and soft segment shear moduli:

$$\ln G = \varphi_H \ln G_H + (1 - \varphi_H)\ln G_S \tag{7}$$

We see that the shear modulus is predicted to be independent of the degree of phase mixing if G_H and G_S remain constant. This explains the results in Fig. 4. There is no significant change in tensile modulus when the degree of phase mixing varies through change only in MD, while DI and CE remain the same. There is no a priori reason to expect G_H or G_S to vary when only the MD changes. Note that all three soft segments have the same molar mass M_S and hence would have the same rubber elastic modulus if crosslinked at their ends.

Secondly, predictions from equation (7) may be compared with measurements of tensile modulus to estimate changes that occur in the hard and soft phase properties, as the chemical and physical structures of the TPUs vary. Fig. 6 shows contours of calculated tensile modulus E plotted versus the hard and soft phase shear moduli, according to equation (7), with $\nu = 0.5$ and $\varphi_H = 0.354$ (the mean hard segment volume fraction). It is possible to place some bounds on the ranges of hard and soft phase moduli. For example, all three macrodiols are above their glass transition at room temperature. Since they all have molar mass $M_S = 2000$, if the hard segments at their ends acted as simple crosslinks, this would lead to an intrinsic soft segment shear modulus $G_S = \rho RT/M_S = 1.2$ MPa at room temperature for all the polymers, according to the affine chain theory of rubber elasticity (we neglect here the small differences in density). But this assumes the chains are completely free of constraint except from crosslinks. In

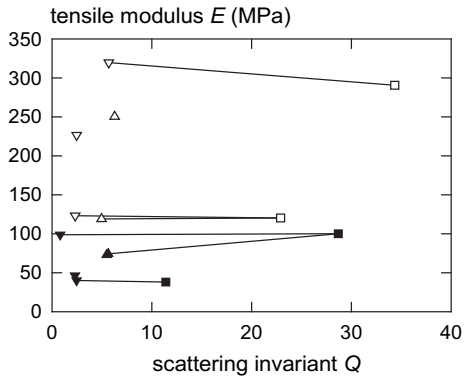

Fig. 4. Tensile modulus versus SAXS invariant Q (in arbitrary units). Filled symbols = MDI-based polymers; open symbols = DBDI-based polymers. Symbol shapes indicate the macrodiol: ∇ PEA; □ PTHF; Δ PBA. Lines are only to guide the eye: they link materials differing only in their macrodiol.

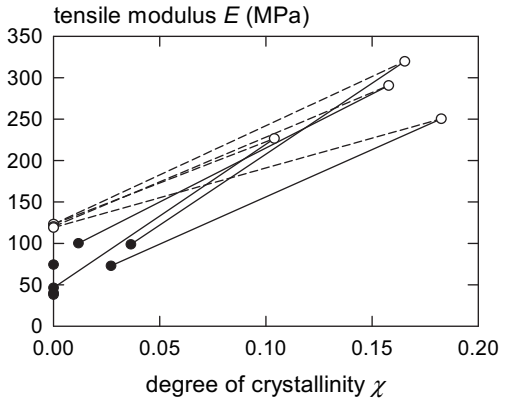

Fig. 5. Tensile modulus versus degree of crystallinity deduced from WAXS. Filled symbols = MDI-based polymers; open symbols = DBDI-based polymers. Lines are only to guide the eye: they link materials differing only in di-isocyanate (full lines) or in chain extender (dashed lines).

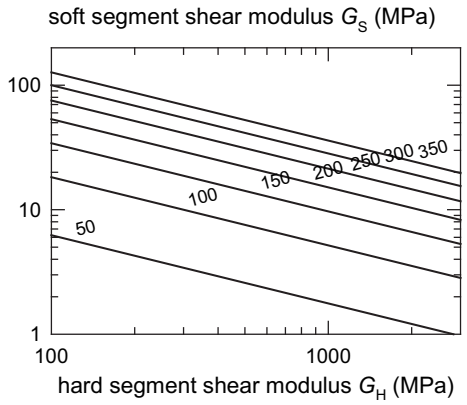

Fig. 6. Contours of tensile modulus (MPa) for a TPU with hard segment volume fraction $\varphi_H = 0.354$ and Poisson's ratio $\nu = 0.5$, according to the empirical log law for shear modulus of a two-phase composite material (equation (7)).

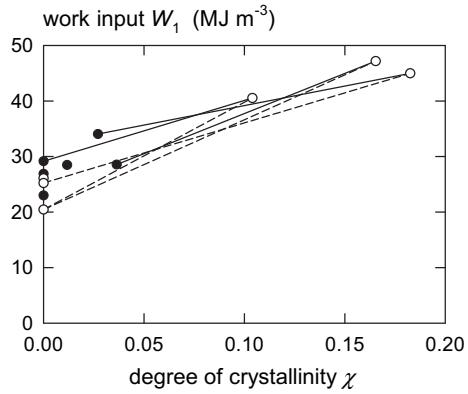

Fig. 8. First cycle work input W_1 on loading to $e = 3$, plotted versus degree of crystallinity. Filled symbols = MDI-based polymers; open symbols = DBDI-based polymers. Lines are only to guide the eye: they link materials differing only in di-isocyanate (full lines) or in chain extender (dashed lines).

the TPUs this must represent a *lower* bound on G_S, since the chains are subject to additional constraint from the excluded volume of, and connectivity to, the hard domains as noted in Section 3.1. Thus a higher value is expected for G_S.

Similarly, in the absence of any phase mixing, the hard phase is a hydrogen-bonded glassy or semicrystalline polymer. Experience of other polymers suggests that $G_H \approx 1000$ MPa at room temperature. But this is a typical value for a macroscopic sample of polymer. In the TPUs it must represent an *upper* bound on G_H, since in this case the hard segments are confined to such small domains that a large fraction of them reside at the particle surfaces, adjacent to the more mobile matrix, again as shown above in Section 3.1. So a lower value is expected for G_H.

Fig. 6 provides a chart on which we may place the various materials. Consider the MDI-based polymers, with E in the range 39–86 MPa. It may be seen that these values could be achieved with a range of combinations of G_H and G_S, varying from a glassy value of G_H combined with almost no increase of G_S above its lower bound, to a substantially reduced G_H (indicating an unusually compliant glass) combined with significant increase in G_S. Consider now the DBDI-based, but non-crystalline polymers with $E = 122$–138 MPa. Fig. 6 shows that in this case there is definitely substantial soft-phase stiffening, by a factor of at least 6. It can be explained by the closer packing and hydrogen bonding of DBDI-based hard segments in hard domains, causing higher constraint at the ends of soft segments. Finally, the DBDI-based semicrystalline polymers with $E = 185$–320 MPa must have even higher soft-phase stiffening. In the most extreme case G_S must be at least ca 20 MPa. Clearly, crystallization in the hard domains causes severe constraint on the soft phase segments because of molecular connectivity between the phases.

3.2.2. First cycle work input, unrecovered strain and hysteresis

Figs. 7 and 8 show the 1st cycle work input W_1 plotted versus scattering invariant Q and degree of crystallinity χ. W_1 is a measure of the mean flow stress during first extension to $e = 3$. If the soft phase is rubberlike with mobile soft segments (i.e. with minimal phase-mixing), the origin of the flow stress and hence W_1 is expected to be plastic flow in only the hard domains. With phase-mixing, the hard phase flow stress will decrease as more mobile soft segments penetrate the hard domains, but at the same time the soft matrix will develop a resistance to flow, as relatively low mobility hard segments are now interspersed among the soft segments. These two effects will act in opposition, and Fig. 7 shows that they approximately cancel: there is no trend of varying W_1 with change in degree of phase separation (indicated by Q). As with the modulus, however, Fig. 8 reveals a significant increase in W_1 with increasing degree of crystallinity. This is readily explicable, since more efficient molecular packing is expected to cause an increase in the activation barrier, and hence the driving stress and hence W_1, associated with the flow process. Interestingly, unlike the

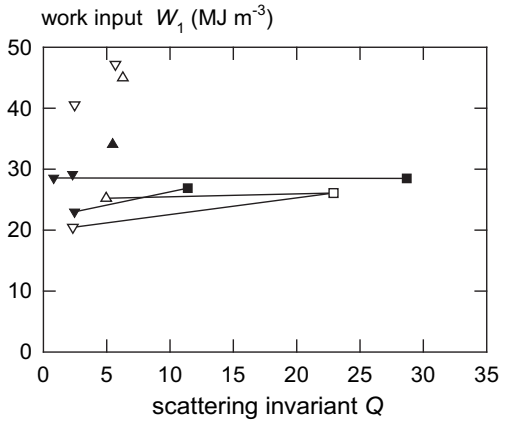

Fig. 7. First cycle work input W_1 on loading to $e = 3$, plotted versus SAXS invariant Q. Symbols as in Fig. 4. Lines are only to guide the eye: they link materials differing only in their macrodiol.

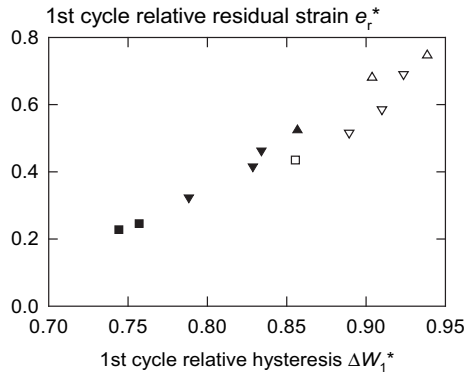

Fig. 9. First cycle relative residual strain on loading/unloading to $e = 3$, plotted versus first cycle relative hysteresis, showing correlation and trends with respect to choice of DI and MD. Symbols as in Fig. 4.

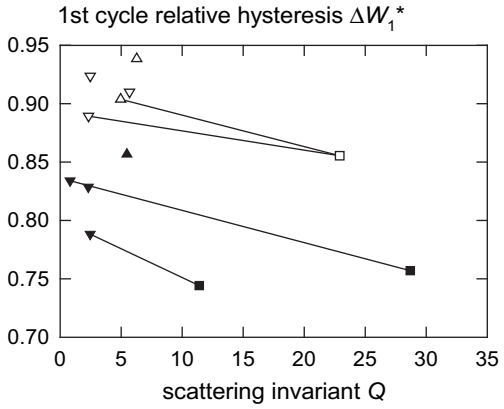

Fig. 10. First cycle relative hysteresis on loading/unloading to $e = 3$, plotted versus SAXS invariant Q. Symbols as in Fig. 4. Lines are only to guide the eye: they link materials differing only in their macrodiol.

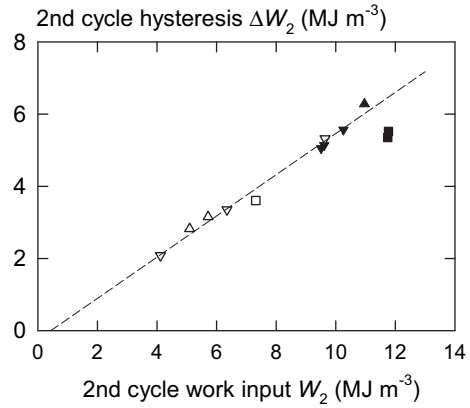

Fig. 12. Hysteresis versus work input for the second load/unload cycle to $e = 3$. Symbols as in Fig. 4. The dashed line is a linear regression through all points except those of Pu7 and Pu8.

case of the modulus, there is no evidence in Fig. 8 for DBDI-based hard domains requiring a higher flow stress than MDI domains in the absence of crystallinity.

Since the TPUs are candidates for use as thermoplastic elastomers, the degree of strain recovery (or its converse, permanent set) is of great practical interest. The examples in Fig. 3 illustrate the fact that strain recovery varies widely among these materials. It is apparent that residual strain is a consequence of the unloading stress-strain curve deviating from the loading curve, in other words it is a consequence of hysteresis. For this reason, the data in columns 4 and 5 of Table 2 are closely related. In Fig. 9 relative residual strain e_r^* is plotted versus relative first cycle hysteresis ΔW_1^*, and they can be seen to be well correlated across the range of materials. This figure also reveals two important trends with respect to the effects of chemical composition on first cycle hysteresis. Firstly, MDI-based polymers show substantially lower residual strain and relative hysteresis than the corresponding DBDI-based polymers. Secondly, for a given DI, polymers with PTHF as MD show lower residual strain and hysteresis than the corresponding polymers with PEA or PBA as MD.

The relation between ΔW_1^* and physical structure is revealed in Figs. 10 and 11. Fig. 10 shows that it tends to fall when phase separation increases, and this is why the PTHF-based polymers show the lowest hysteresis. Conversely, ΔW_1^* is found to increase with degree of crystallinity, as shown in Fig. 11. To explain these trends in the response to loading followed by *unloading* requires an understanding of the structural damage taking place during first loading. A suggestion is offered in the Discussion below.

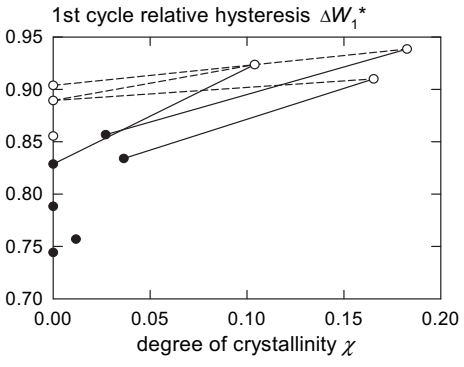

Fig. 11. First cycle relative hysteresis on loading to $e = 3$, plotted versus degree of crystallinity. Filled symbols = MDI-based polymers; open symbols = DBDI-based polymers. Lines are only to guide the eye: they link materials varying only in diisocyanate (full lines) or in chain extender (dashed lines).

3.2.3. Second cycle work input and hysteresis

The example stress-strain curves in Fig. 3 illustrate the dramatic difference in response of these materials in second and subsequent load/unload cycles to a given strain level, as compared to the first cycle. Clearly, damage occurs during the first cycle. The second cycle response is effectively that of a new material. The work input W_2 and hysteresis ΔW_2 on the second cycle are included as columns 6 and 7 in Table 2, as obtained from the cyclic experiments of Phase 1. They are plotted one versus the other in Fig. 12, for all the 12 materials that could withstand cycling to $e_{max} = 3$. The remarkable feature of this graph is that there appears to be a single linear relationship between ΔW_2 and W_2 encompassing all the materials *except* Pu7 and Pu8: the MDI-based polymers with highest phase separation. The dashed line shown is a linear regression through all the points except these two, with $R^2 = 0.986$, as follows (uncertainties quoted are the standard errors of the coefficients):

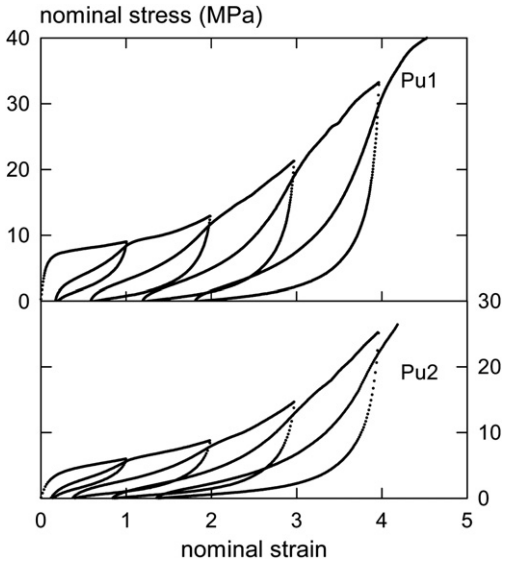

Fig. 13. Stress versus strain for "pseudo-cyclic" loading of two TPU materials at nominal strain-rate 0.03 s^{-1} Pu1 and Pu2 are both based on MDI and PEA but differ in their chain extender. Pu1 has slight crystallinity (4%) while Pu2 is amorphous.

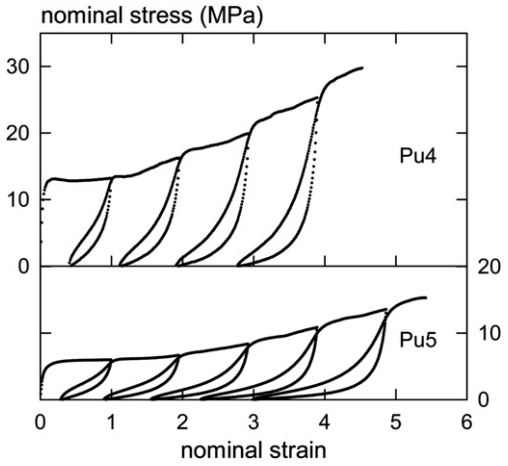

Fig. 14. Stress versus strain for "pseudo-cyclic" loading of two TPU materials at nominal strain-rate 0.03 s^{-1} Pu4 and Pu5 are both based on DBDI and PEA, but differ in their chain extender. Pu4 has significant crystallinity (17%) while Pu5 is amorphous.

$$\Delta W_2 = (0.57 \pm 0.02) W_2 - (0.25 \pm 0.20)\ \mathrm{MJm^{-3}} \quad (8)$$

However, the various materials appear at widely differing positions along this line. It is interesting to note that W_2 (and therefore ΔW_2) tends to be lowest for the DBDI-based materials, irrespective of their crystallinity. The reason for the highly phase-separated materials Pu7 and Pu8 having a slightly lower relative 2nd cycle hysteresis $\Delta W_2/W_2$ than all the other polymers is unknown at this stage, but it is interesting to note that these materials also showed the lowest relative hysteresis in the first cycle (see Fig. 10 and Table 2).

3.3. Mechanical tests – Phase 2

Examples of stress–strain curves obtained in the more complex pseudo-cyclic experiments of Phase 2 are shown in Figs. 13–15, where pairs of materials are compared. Fig. 11 compares Pu1 and Pu2. These materials are closely related, both being based on MDI and PEA, and differing only in chain extender (see Table 1). However Pu1 has a small degree of hard phase crystallinity (4%), while Pu2 is amorphous. It is interesting to note the differences in the curves: the slight degree of crystallinity in Pu1 clearly increases the stress levels reached throughout the test, and gives a much higher modulus (see also Table 2). Fig. 14 compares the two DBDI-based polymers Pu4 and Pu5. These both have PEA as MD, but differ

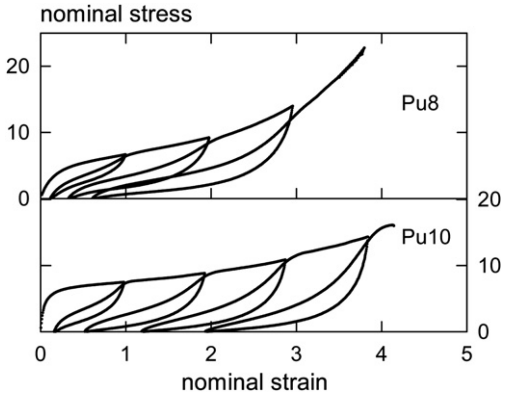

Fig. 15. Stress versus strain for "pseudo-cyclic" loading of two TPU materials at nominal strain-rate 0.03 s^{-1} Pu8 is PTHF + DEG + MDI, Pu10 is PTHF + DEG + DBDI. Neither has detectable crystallinity. Both have significant phase separation.

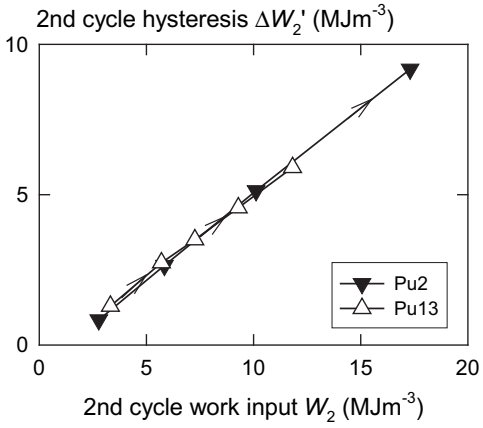

Fig. 16. Hysteresis versus work input for load/unload cycles to increasing e_{max}, in the pseudo-cyclic experiments of Phase 2, for materials Pu2 and Pu13. Arrows indicate the direction of increasing e_{max}.

in CE. Pu4 has EG as chain extender and therefore has significant crystallinity (17%), while Pu5 has DEG as chain extender and therefore has no detectable crystallinity. The effect of crystallinity in Pu4 is clearly to cause a large increase in stress throughout, and to increase the residual strain on each cycle. Fig. 15 compares Pu8 and Pu9, that are both based on PTHF and DEG, but differ in DI. They are both amorphous, and both highly phase-separated. But the presence of DBDI in Pu10 can be seen to increase residual strain in each cycle, and to reduce the rate of strain-hardening compared to Pu8. An equivalent comparison can be made between Pu2 in Fig. 13 and Pu5 in Fig. 14, where the same pattern of differences is visible.

Figs. 13–15 illustrate the fact that stress-strain paths followed in the pseudo-cyclic tests show significant quantitative differences between the materials, although all exhibit the characteristic Mullins effect and varying degrees of residual strain, increasing with e_{max}. It is interesting, therefore, to discover whether the second cycle responses at each strain level reflect the remarkable degree of commonality seen in Phase 1 experiments. As examples,

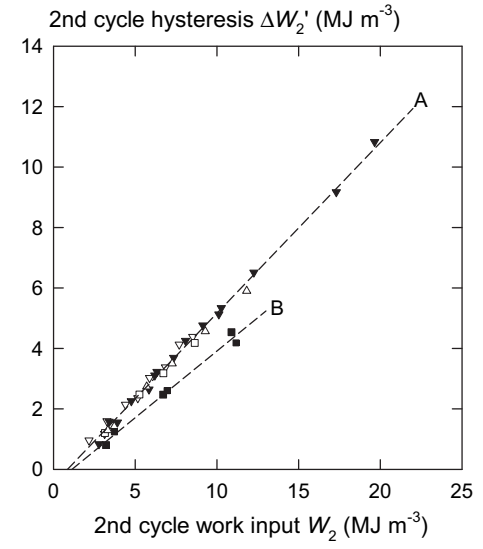

Fig. 17. Hysteresis versus work input for second cycle load/unload to increasing e_{max}, in the pseudo-cyclic experiments of Phase 2. Symbols are as in Fig. 4. The two dashed lines are linear regressions through data for sub-sets of the materials: A (all materials except Pu7 and Pu8), and B (Pu7 and Pu8, both shown as ■).

Fig. 16 shows second cycle hysteresis and work input for two materials: Pu2 (MDI + DEG + PEA) and Pu13 (DBDI + DEG + PBA). For each material, $\Delta W_2'$ is plotted versus W_2 in successive cycles. Arrows indicate the direction of increasing e_{max}. This graph reveals two surprising features. First, for each material the points appear to fall on a straight line, with a single direction of travel away from the origin with increasing e_{max}. Second, data for both materials (with differing DI and MD) appear to lie on the *same* straight line.

It is of interest to know whether this commonality extends to *all* the cycles for *all* the materials. Fig. 17 therefore shows all the measurements of W_2 and $\Delta W_2'$: data for all the ten materials included in Phase 2 (materials 9, 11, 12 and 14 failed before completion of at least three cycles), and all cycles in their tests.

Fig. 17 confirms the trend seen already in Fig. 12, but with a much larger data set. The data for *all* the materials except Pu7 and Pu8, for *all* loading cycles, lie on a common straight line. Moreover, in every case, the sequence of points was found to be the same as in Fig. 16: towards higher W_2 with increasing maximum strain. Materials Pu7 and Pu8 behave similarly, but lie on a different line. These observations may be quantified by fitting linear regressions through the data points. Thus the data for eight materials Pu1, Pu2, Pu3, Pu4, Pu5, Pu6, Pu10 and Pu13 (34 data points in total) fitted the following relation with $R^2 = 0.995$ (line A in Fig. 17):

$$\Delta W_2' = (0.565 \pm 0.007) W_2 - (0.48 \pm 0.05)\ \mathrm{MJm^{-3}} \quad (9)$$

The data for materials Pu7 and Pu8 (7 points only) fitted the different relation with $R^2 = 0.988$ (line B in Fig. 17):

$$\Delta W_2' = (0.44 \pm 0.02) W_2 - (0.50 \pm 0.19)\ \mathrm{MJm^{-3}} \quad (10)$$

Thus we see the pattern reported in Fig. 12 is confirmed and greatly extended in its reach. For most of the materials in the present study there is a common linear relationship between second cycle hysteresis and second cycle work input, and this relationship is independent of e_{max} reached on the first cycle. Note that the linear relations described by equations (8) and (9) are identical to within the standard errors of the coefficients. However, a sub-set of the present materials (Pu7 and Pu8) follow a different relation, characterized by lower relative second cycle hysteresis.

4. Discussion

The results presented above reveal a dramatic difference in response between first loading to a given deformation, and second and subsequent loadings. The model TPUs studied in this work showed large, systematic variations in *first* loading response – as quantified by tensile modulus, work input, hysteresis and unrecovered strain – depending on their chemical structure and molecular packing. But on *second* loading to the same strain they showed a remarkable degree of uniformity in their relative hysteresis. The clear conclusion is that first loading causes significant damage to the initial structure, such that second loading corresponds to deformation of a new structure. Moreover, whereas the initial physical structure varies greatly between the materials, the new structure dominant in second loading must be similar between the materials.

To understand this result we may consult the evidence concerning structural changes during deformation of similar materials, provided by in-situ mechano-calorimetry [20,21], infra-red (IR) spectroscopy [22,23], WAXS and SAXS [24–26]. Although the details differ with the precise chemical composition, some features seem to be common to TPU elastomers.

Several studies have followed deformation of the two-phase structure by means of in-situ SAXS. On first loading, small deformations are accompanied by affine deformation of the arrangement of hard domains, but this is followed after stretching to $e \approx 1$ by a deviation towards reduction of long period d relative to affine deformation [24,25], and possibly even to an absolute reduction in d [24]. In some cases the original isotropic scattering is replaced by a four-point pattern [25]. These observations are all explained in terms of breakage of the original hard domains into smaller units during plastic deformation [24,25]. Simultaneously, calorimetric measurements of heat flux, combined with work input, indicate a significant increase in internal energy [20] associated with the less efficient molecular packing of hard segments, once the original two-phase structure starts to break up. This might be thought to suggest a reduction in H-bonding during deformation, but in-situ IR spectroscopy suggests otherwise: the density of H-bonds appears to be independent of strain [27]. Thus, if H-bonds are broken during deformation, new bonds must be formed rapidly on the time-scale of straining. Another interesting observation is the progress of orientation of the various bonds identifiable in IR spectra obtained during straining. Initially the chain orientation as indicated by >N–H and urethane or urea >C=0 groups (i.e. the hard segments) orients perpendicular to direction of extension, while the chain axes of soft segments align parallel to the direction of extension. But beyond $e \approx 1$–2, the hard segments rotate and their chain direction follows that of soft segments, parallel to the direction of extension [23]. This may also be interpreted plausibly in terms of breakage and re-reformation of H-bonds.

On subsequent cycling, within the envelope of previous strains, a totally different pattern has been observed. In-situ SAXS simultaneous with cyclic deformations showed reversible movements of unchanged four-point patterns, although the movements were in opposite directions for two variants on the same TPU, with monodisperse or polydisperse hard segments [26]. Meanwhile, in-situ IR studies simultaneous with pseudo-cyclic experiments of the type in Phase 2 of this work, showed that the orientation pattern of hard segment and soft segment portions of chains was also reversible [23]. Calorimetry during subsequent loading of TPUs with hard segment fractions similar to the polymers of the present study showed that there was no increase in internal energy [21], consistent with no further structural breakdown.

Combining such structural information with results from the present work, a plausible picture of deformation in TPU elastomers emerges. In small deformations below the yield stress, the elastic response is that of a two-phase composite material. The soft matrix responds with a stiffness higher than that of a homogeneous crosslinked elastomer with the soft segment composition, because of constraint from the excluded volume of, and molecular connectivity to, the hard domains, especially so when the hard domains are semicrystalline, and possibly because of some phase mixing with hard segments. At strains beyond yield, break-up of the two-phase structure commences. Bonart and Muller-Riederer suggested how this could proceed by sliding of hard segments relative to their neighbours within the hard domains [1,28]. There are two likely consequences. (I) the sliding could lead to irreversible deformation and hence residual strain, and (II) the sliding could lead to stripping of segments from the hard domains to provide new soft matrix in series with the hard domains, as suggested by Kilian and co-workers [29]. Both these processes would be facilitated by the small sizes of the particles. As noted in Section 3.1, a large proportion of hard segment monomers lies at the surfaces of the hard domains, and therefore must be relatively weakly bound. On unloading, and subsequent re-loading, while the stress remains below the flow stress of the hard domains, the structure is expected to remain constant and reversible deformation to occur. Since the newly-created soft phase is much more compliant than the hard domains and is coupled in series with them, the reversible

deformation occurs essentially entirely within this soft phase, characterized by much lower stiffness and lower hysteresis than the original structure. If the new (series-coupled) structure is loaded up to the flow stress, structural break-up resumes.

This description accounts qualitatively for the characteristic constitutive response seen in the present work, and provides a basis for understanding its dependence on chemical and physical structure. But the new results also add an unexpected twist. The reproducibility of relative hysteresis on second and subsequent loading indicates that the new series-coupled soft phase, formed by stripping segments from the hard domains, has almost constant relative hysteresis, independent of the strain level at which it is formed. Moreover it is (with two minor deviations among the range of polymers studied) independent of chemical composition of DI, CE and MD, when the MDs are of equal length and HS fractions are equal. Why the small sub-set Pu7 and Pu8, based on MDI but with highest phase segregation should have a slightly lower relative hysteresis than the others remains unclear. However, one could speculate that it results from a lower degree of intermolecular H-bonding being achieved in the new soft phase (because of the combination of (a) absence of ester >C=0 groups and (b) the relatively less mobile MDI).

To understand the relative first cycle hysteresis $\Delta W_1{}^*$ we need to consider the processes of both first loading and unloading. In terms of the description above, its value is expected to be sensitive to the relative importance of the two damage processes identified: (I) and (II). Thus its reduction with replacement of DBDI by MDI, or with increasing phase separation (Figs. 9 and 10) could be caused by increase in contribution from process II, relative to process I, in these cases, presumably because of weaker binding of segments to the hard phase.

The explanation offered above for the Mullins effect in these materials differs in an important respect from the model proposed by Qi and Boyce [3]. That model invokes parallel coupling between the hard domains and (strain amplified) soft matrix, and explains the Mullins effect in terms of a reduction of strain amplification in the matrix with increasing strain. In such a parallel-coupled structure, second and subsequent cycles of loading would involve cyclic deformation of the hard phase in addition to the rubbery soft phase. This appears to be inconsistent with the structural studies reported above, and not to be reconcilable with the new results, since the two hard phases show greatly differing relative hysteresis (as seen on the first cycle) while there is remarkable commonality of relative hysteresis in second and subsequent cycles.

5. Conclusions

A systematic study has been made of structural features and cyclic tensile responses of a series of fourteen TPU elastomers, in which hard segment mass fraction and soft segment molar mass were held constant at approximately 39% and 2000 respectively, but the DI, MD and CE were varied. Two DIs, three MDs and three CEs were included. On first loading, the tensile modulus and work input at 300% strain were found to increase significantly with increase in hard phase degree of crystallinity, achieved primarily by use of DBDI (with EG or BG as chain extender) instead of MDI as di-isocyanate. This may be explained by increase in constraint on the soft phase at the hard domain boundaries, and by increased activation barrier for plastic flow in the hard phase respectively. However the same two quantities were found to be independent of the degree of phase segregation. In both cases, although phase mixing is expected to give different phase properties, it appears the effects on the two phases approximately cancel and no significant overall change is observed.

The following is a plausible picture of events during strain cycling beyond yield, consistent with in-situ structural evidence and present results. During first loading, break-up of the hard domains occurs, producing new soft phase coupled in series with the remaining hard phase, as suggested by Kilian and co-workers. During unloading and subsequent re-loading, it is this more compliant phase that dominates the deformation. Such a description explains why second and subsequent loading/unloading inside the envelope of previous maximum strain gave responses totally different from first loading. They were characterized by much lower stiffness and hysteresis (the Mullins effect). It also sheds light on the most remarkable discovery from the present work: the apparently almost unique linear relation between second cycle hysteresis and work input. This relation is independent of the previous maximum strain reached, and it is *almost* independent of choice of DI, MD and CE. Curiously, two polymers – the best phase–separated polymers based on MDI – showed slightly lower second cycle hysteresis. In terms of the Kilian hypothesis, these results indicate the mechanical response of the new soft phase is remarkably independent of the chemical structure of the TPU if, as in the present work, the hard segment fraction and soft segment chain length are held constant.

One aspect of the present results – relative first cycle hysteresis – depends upon the responses of both the initial structure and of the new soft phase, and is also sensitive to the precise mechanism of flow and break-up of the hard domains. It was observed to reduce with increasing phase segregation and with replacing DBDI with MDI as di-isocyanate. In terms of the picture of structural break-up invoked above, this suggests that in such cases there is relatively more stripping of segments from hard domains, and less plastic deformation of them. A possible explanation is weaker binding of segments at the hard domain boundaries.

Acknowledgements

This work was supported by NATO Collaborative Linkage Grant CBP.EAP.CLG.981805. The authors are grateful to Mr Victor Prisacariu for assistance in the processing of data.

References

[1] Bonart R, Müller-Riederer G. Colloid and Polymer Science 1981;259:926–36.
[2] Buckley CP, Prisacariu C, Caraculacu A, Martin CM. In: Austrell P-E, Hari L, editors. Constitutive models for rubber IV. London: Taylor and Francis; 2005. p. 465–70.
[3] Qi HJ, Boyce MC. Mechanics of Materials 2005;37:817–39.
[4] Petrovic ZS, Ferguson J. Progress in Polymer Science 1991;16:695–836.
[5] Prisacariu C, Agherghinei I. Journal of Macromolecular Science Part A 2000; A37:785–806.
[6] Dietrich D, Hespe H. In: Oertel G, editor. Polyurethane Handbook. Munich: Hanser Publishers; 1985. p. 37–53.
[7] Seefried CG, Koleske JV, Critchfield FE. Journal of Applied Polymer Science 1975;19:2493–502.
[8] Trappe G. Polyurethane elastomers. In: Buist JM, Gudgeon H, editors. Advances in polyurethane Technology. London: MacLaren and Sons; 1968. p. 25–33.
[9] Waletzko RS, James Korley LT, Pate BD, Thomas EL, Hammond PT. Macromolecules 2009;42:2041–53.
[10] Prisacariu C, Olley RH, Caraculacu A, Bassett DC, Martin CM. Polymer 2003;44:5407–21.
[11] Prisacariu C, Buckley CP, Caraculacu A. Polymer 2005;46:3884–94.
[12] Prisacariu C, Scortanu E. High Performance Polymers 2008;20:117–25.
[13] Gower LA, Wang TLD, Lyman DJ. Journal of Biomaterials Science, Polymer Edition 1995;6:761–73.
[14] Bonart R, Morbitzer L, Rinke H, Kolloid-Z. uZ. Polymere 1970;240:807–19.
[15] Saiani A, Rochas C, Eeckhaut G, Daunch WA, Leenslag J-W, Higgins JS. Macromolecules 2004;37:1411–21.
[16] Alexander LE. X-Ray diffraction Methods in polymer Science. New York: Wiley-Interscience; 1969.
[17] Hashin Z, Shtrickman S. Journal of Mechanics and Physics of Solids 1963;11:127–40.
[18] Christensen RM. Mechanics of composite materials. New York: Wiley; 1979.

[19] Gray RW, McCrum NG. Journal of Polymer Science, Part A-2 1969;7:1329–55.
[20] Godovsky YK, Bessanova NP, Mironova NN. Colloid and Polymer Science 1986; 264:224–30.
[21] Godovsky YK, Bessanova NP, Mironova NN. Colloid and Polymer Science 1989; 267:414–20.
[22] Moreland JC, Wilkes GL, Turner RB. Journal of Applied Polymer Science 1991; 43:801–15.
[23] Yeh F, Hsiao BS, Sauer BB, Michel S, Siesler HW. Macromolecules 2003; 36:1940–54.
[24] Desper CR, Schneider NS, Jasinski JP, Lin JS. Macromolecules 1986;18:2755–61.
[25] Blundell DJ, Eeckhaut G, Fuller W, Mahendrasingam A, Martin C. Polymer 2002;43:5197–207.
[26] Blundell DJ, Eeckhaut G, Fuller W, Mahendrasingam A, Martin C. Journal of Macromolecular Science, Part B 2004;B43:125–42.
[27] Seymour RW, Estes GM, Cooper SL. Macromolecules 1970;3:579–83.
[28] Bonart R. Polymer 1979;20:1389–403.
[29] Enderle HF, Kilian H-G, Heise B, Mayer J, Hespe H. Colloid and Polymer Science 1986;264:305–22.